Journal of Quantitative Spectroscopy & Radiative Transfer 255 (2020) 107263

Contents lists available at ScienceDirect

Journal of Quantitative Spectroscopy & Radiative Transfer

journal homepage: www.elsevier.com/locate/jqsrt

Line positions and intensities of the ν_4 band of methyl iodide using mid-infrared optical frequency comb Fourier transform spectroscopy

Ibrahim Sadiek[a,1], Adrian Hjältén[a], Francisco Senna Vieira[a,2], Chuang Lu[a], Michael Stuhr[b], Aleksandra Foltynowicz[a,*]

[a] Department of Physics, Umeå University, 901 87 Umeå, Sweden
[b] Institute of Physical Chemistry, University of Kiel, 24118 Kiel, Germany

ARTICLE INFO

Article history:
Received 7 July 2020
Revised 14 August 2020
Accepted 16 August 2020
Available online 18 August 2020

Keywords:
Methyl iodide
High-resolution spectroscopy
Optical frequency comb
Fourier transform spectroscopy

ABSTRACT

We use optical frequency comb Fourier transform spectroscopy to measure high-resolution spectra of iodomethane, CH_3I, in the C–H stretch region from 2800 to 3160 cm^{-1}. The fast-scanning Fourier transform spectrometer with auto-balanced detection is based on a difference frequency generation comb with repetition rate, f_{rep}, of 125 MHz. A series of spectra with sample point spacing equal to f_{rep} are measured at different f_{rep} settings and interleaved to yield sampling point spacing of 11 MHz. Iodomethane is introduced into a 76 m long multipass absorption cell by its vapor pressure at room temperature. The measured spectrum contains three main ro-vibrational features: the parallel vibrational overtone and combination bands centered around 2850 cm^{-1}, the symmetric stretch ν_1 band centered at 2971 cm^{-1}, and the asymmetric stretch ν_4 band centered at 3060 cm^{-1}. The spectra of the ν_4 band and the nearby $\nu_3+\nu_4-\nu_3$ hot band are simulated using PGOPHER and a new assignment of these bands is presented. The resolved ro-vibrational structures are used in a least square fit together with the microwave data to provide the upper state parameters. We assign 2603 transitions to the ν_4 band with a standard deviation (observed – calculated) of 0.00034 cm^{-1}, and 831 transitions to the $\nu_3+\nu_4-\nu_3$ hot band with a standard deviation of 0.00084 cm^{-1}. For comparison, in the earlier work using standard FT-IR with 162 MHz resolution [Anttila, et al., J. Mol. Spectrosc. 1986; 119:190–200] 1830 transition were assigned to the ν_4 band, and 380 transitions to the $\nu_3+\nu_4-\nu_3$ hot band, with standard deviations of 0.00083 cm^{-1} and 0.0013 cm^{-1}, respectively. The hyperfine splittings due to the ^{127}I nuclear quadrupole moment are observed for transitions with $J \leq 2 \times K$. Finally, intensities of 157 isolated transitions in the ν_4 band are reported for the first time using the Voigt line shape as a model in multispectral fitting.

1. Introduction

Atmospheric monitoring of photochemically active substances such as halogenated volatile organic compounds (HVOCs) is essential for modeling the natural cycling of climate relevant trace gasses [1]. Iodomethane (CH_3I) –a naturally occurring HVOC – is classified by the World Metrology Organization (WMO) as a very short-lived substance (VSLS), i.e., a trace gas with a local lifetime comparable to or shorter than the tropospheric transport time scale [2], and hence its distribution is non-uniform in the troposphere. Despite the fact that naturally produced CH_3I has a very low atmospheric mixing ratio of 0.1 – 2 parts-per-trillion (ppt) [3], it is an important carrier of iodine from the ocean to the atmosphere and plays a crucial role in the chemistry of the atmosphere. When it is photodissociated by UV light, it can contribute to aerosol formation in the troposphere [4]. Despite its associated risk of exposure to workers and residents, iodomethane is still used in several industrial and agricultural applications, e.g., as a synthetic agent in organic synthesis [5] or a fumigant in buildings and soils [6,7]. The use of iodomethane as an agricultural pesticide was promoted following the control of methyl bromide for such purposes under the Montreal Protocol in 1989 [8]. In nuclear power plants, the possible emission of radioactive iodine in the form of methyl iodide during a core melt accident is a major concern [9]. Relevant to all of these applications is the capability to install suitable leak detectors as well as to monitor personal exposure limits, where current occupational safety guidelines set

* Corresponding author.
E-mail address: aleksandra.foltynowicz@umu.se (A. Foltynowicz).
[1] Currently at Leibniz Institute for Plasma Science and Technology (INP), 17489 Greifswald, Germany
[2] Currently at VTT Technical Research centre of Finland Ltd, Tekniikantie 1, 02150 Espoo, Finland

https://doi.org/10.1016/j.jqsrt.2020.107263

the personal exposure limit to 0.3 – 5 parts-per-million (ppm), depending on the regulatory authority [10].

Currently, the detection of CH_3I is based on gas chromatography coupled with mass spectrometry or electron capture detection (GC–MS/ECD). These techniques allow only for discrete measurements, require calibration, and are time consuming (i.e., several tens of minutes per sample). Thus, they are not suitable for workspace monitoring, leak detection or process studies that examine rapid changes associated with natural production and loss processes. Laser-based absorption techniques should, in principle, be able to overcome the limitation of the GC–MS/ECD techniques as they provide non-invasive sensing with fast acquisition and high-sensitivity. So far, there is only one laser-based absorption study [11], using mid-infrared continuous wave cavity ring-down spectroscopy (mid-IR cw-CRDS), where CH_3I from a tank-purging experiment was detected at the ^{r}R2(15) ro-vibrational absorption transition. A limit of detection of 15 parts-per-billion (ppb) was achieved, sufficient for practical applications where ppm mixing ratios are expected, such as workplace monitoring. A major challenge that limits the applicability of laser-based absorption techniques, particularly those based on narrowband cw lasers, is the potential interference of other absorbing molecules (i.e., the so-called absorption cross-sensitivity). Therefore, broadband high-resolution measurements of mid-IR spectra of CH_3I are a prerequisite for the selection of a suitable detection range, and for accurate determination of band parameters and spectral line parameters.

There exist several microwave [12,13] and Doppler-free double-resonance [14,15] spectroscopic studies of the ground and first excited states of CH_3I. In the infrared region, the molecule has been a subject of numerous studies concerning mostly the line positions of its vibrational bands: ν_1 [16], ν_2 [17], ν_3 [18], ν_4 [19,20], ν_5 [21], and ν_6 [22]. Line positions of several overtone and combination bands were also investigated [22,23]. In contrast, there exist only a few studies of the line intensities of these bands of CH_3I. To the best of our knowledge, high-resolution studies of the line intensities exist only for the ν_6 and the $2\nu_3$ bands [24,25] and for some lines of the ν_5 and $\nu_3+\nu_6$ bands [26]. There are low-resolution measurements of the overall band intensities of the six fundamental vibrations [27,28], and *ab initio* computed intensities of its fundamental bands [29].

The ν_4 band, centered at 3060 cm^{-1}, is interesting for spectroscopic detection as it lies in the range where many laser sources became recently available, but it is rather understudied. The two previous studies [19,20] used standard Fourier transform infrared spectroscopy (FT-IR) with a resolution of ~0.0054 cm^{-1} (~160 MHz), which is larger than the Doppler width of CH_3I at 3000 cm^{-1} and 296 K (96 MHz), and provided line positions but no information about the line intensities. In the first measurements of the ν_4 band by Connes et al. [19] more than 500 lines were fitted with a standard deviation (obs. – calc.) of the assigned lines of 0.005 cm^{-1}. However, only limited parts of the band were used and striking perturbations, causing irregularities in the sub-bands $^{P}Q_6$ and $^{R}Q_5$ – $^{R}Q_7$ remained unexplained. Later on, Anttila et al. [20] reanalyzed the ν_4 band and were able to explain the observed irregularities in rotational structures of the sub-bands as a consequence of Coriolis and Fermi resonances with combination band levels. Overall, 1850 transitions were assigned by Anttila et al. [20] for the ν_4 band and 380 transitions for the nearby $\nu_3+\nu_4-\nu_3$ hot band, with standard deviations of 0.00083 cm^{-1} and 0.0013 cm^{-1}, respectively.

The scope of this work is to use mid-IR comb-based Fourier transform spectroscopy (FTS) to measure high-resolution broadband spectra of iodomethane ($^{12}CH_3I$) in the C–H stretch region from 2800 to 3160 cm^{-1}. The comb-based FTS allows acquisition times orders of magnitude shorter than conventional FT-IR spectroscopy based on incoherent light sources [30]. In addition, by precisely matching the nominal resolution of the FTS to the comb repetition rate [31–33], the comb lines are sampled accurately and high-resolution molecular spectra are measured with no observable instrumental line shape distortions, even when the absorption line widths are narrower than the nominal resolution of the spectrometer. The broadband and the high resolution capability of comb-based FTS allowed us to create a new line list of the ν_4 band and the nearby $\nu_3+\nu_4-\nu_3$ hot band based on available microwave data and the earlier model of Anttila et al. [20], and to observe for the first time the hyperfine splitting due to the large ^{127}I nuclear quadrupole moment in the ν_4 band. Overall, 2603 transitions are assigned for the ν_4 band with a standard deviation of 0.00034 cm^{-1} and 831 transitions are assigned for the $\nu_3+\nu_4-\nu_3$ hot band with a standard deviation of 0.00084 cm^{-1}. Moreover, we report the so far lacking intensities of a first set of 157 well-resolved lines in the ν_4 band using multispectral fitting with the Voigt lineshape function.

2. Experimental setup and procedures

Fig. 1 depicts a schematic of the experimental setup, which consisted of a mid-IR frequency comb, a multipass absorption cell, a Fourier transform spectrometer, and a gas supply system. The mid-IR frequency comb was produced via difference frequency generation (DFG) in a Mg-doped periodically poled lithium niobate (MgO:PPLN) crystal between the output of a high-power 125 MHz Yb-doped fiber laser (Menlo, Orange High Power) and a Raman-shifted soliton generated from the same source in a highly nonlinear fiber (HNLF). The center frequency of the idler was tuned to 2975 cm^{-1}, where the comb has a bandwidth of 360 cm^{-1} and output power of 120 mW. The design and characteristics of this source were presented in detail by Soboń et al. [34]. Three changes were implemented to the DFG source compared to the first demonstration. First, to increase the long term stability of the idler power and center frequency, the single-mode HNLF was replaced by a polarization-maintaining HNLF that allowed achieving the same center wavelength of the Raman-shifted soliton at a lower input pump power. Second, to reduce the intensity noise of the idler, the delay stage in the pump arm was stabilized using an approach similar to the one reported by Silva de Oliveira et al. [35], as shown in the lower part of Fig. 1. A fraction of the idler beam was sampled by a pellicle beamsplitter, dispersed by a diffraction grating, and a selected wavelength region was imaged on a photodetector. The idler intensity noise in the 10–300 kHz bandwidth was measured using a demodulating logarithmic amplifier (DLA). A 7 kHz dither was applied to the pump diode current of the Yb-doped fiber oscillator, and the output of the DLA was demodulated at this frequency using a lock-in amplifier to produce an error signal. A proportional-integral (PI) controller provided a correction signal via a high-voltage amplifier (HVA) to the piezoelectric transducer (PZT) on which the retroreflector in the pump arm was mounted. The correction signal was monitored using a computer and kept within the operating range of the PZT by moving the translation stage on which the retroreflector assembly was mounted. Third, the repetition rate of the comb was stabilized to a tunable direct digital synthesizer (DDS) referenced to a GPS-disciplined Rb oscillator (with a relative stability of 10^{-11} @ 1 s), as shown in the upper left part of Fig. 1. The RF signal at f_{rep} was first mixed with a reference 100 MHz signal from DDS1, and the resulting signal was band-pass filtered at 25 MHz and further mixed with a 25 MHz signal from DDS2. The resulting error signal was fed into a PI controller that acted on the intra-cavity PZT of the Yb-doped fiber oscillator to stabilize the repetition rate. The stepping of f_{rep} during spectral acquisition was done using DDS2. We note that the carrier envelope offset frequency of the DFG source is zero, because both the pump and the signal combs come from the same source.

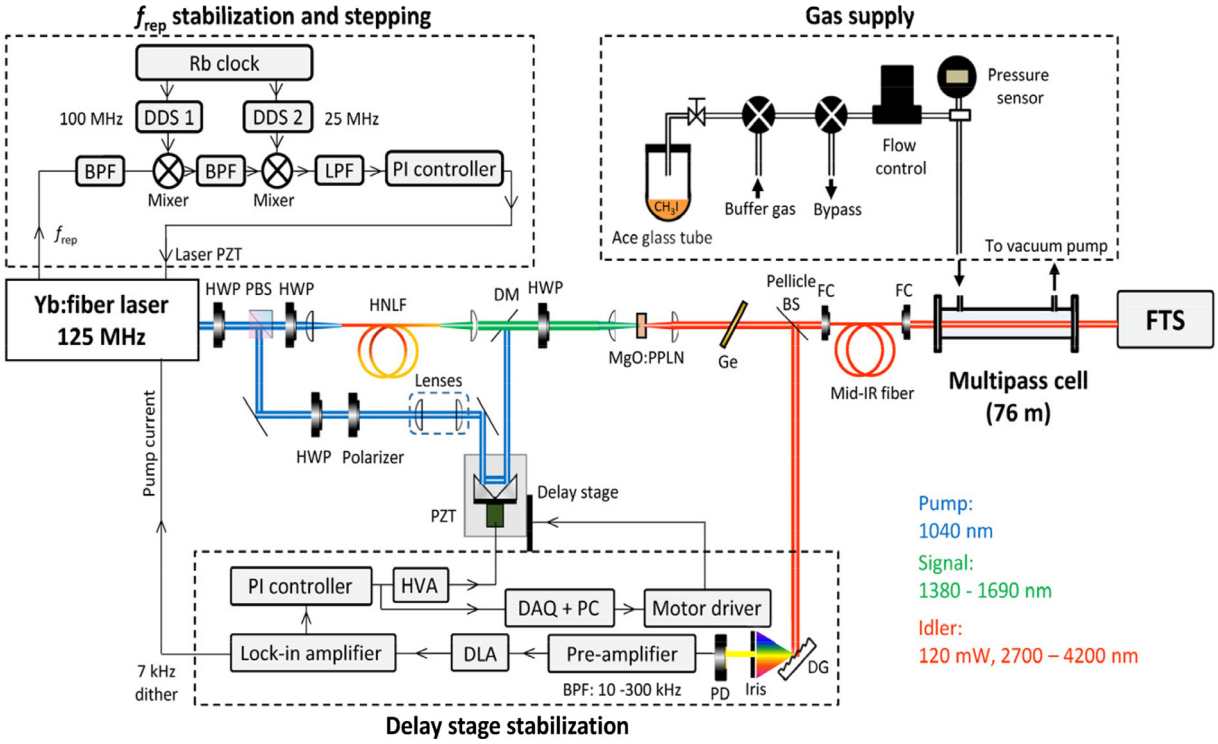

Fig. 1. Schematic of the experimental setup. DDS: direct digital synthesizer, BPF: band pass filter, LPF: low pass filter, PZT: piezoelectric transducer, HWP: half-wave plate, PBS: polarizing beam splitter, HNLF: highly nonlinear fiber, DM: dichroic mirror, MgO:PPLN: Mg-doped periodically poled lithium niobate crystal, Ge: Germanium filter, FC: fiber collimator, FTS: Fourier transform spectrometer, DG: diffraction grating, PD: photodetector, DLA: demodulating logarithmic amplifier, HVA: high voltage amplifier, DAQ+PC: data acquisition card and a personal computer.

The idler beam was led to the absorption cell via a single-mode ZrF_4-BaF_2-LaF_3-AlF_3–NaF (ZBLAN) fiber. The absorption cell was a Herriot type astigmatic cell with 76 m path length (Aerodyne, AMAC-76LW). Analytical grade methyl iodide (Sigma-Aldrich, 99%, containing copper as stabilizer) was used as supplied without further purifications. For all the measurements the sample was contained in an Ace glass tube and was brought into the evacuated gas cells by its vapor pressure, as shown in the upper right part of Fig. 1. The headspace of the sample container was equilibrated and evacuated several times in order to have pure CH_3I gas for the measurements. Dry air was used as a buffer gas. The cell pressure and the gas mixing ratio were controlled by a needle valve and a calibrated pressure transducer (CERAVAC, CTR 101 N) with a specified relative accuracy of 0.15% and readout resolution of 10 μbar. All spectra were recorded at room temperature of (296 ± 0.6) K. The ambient laboratory temperature was monitored by a PT100 platinum resistance thermometer placed in close contact with the measurement cell.

After passing through the absorption cell, the comb beam was coupled into a home-built fast-scanning FTS [36] with a scan speed of 0.4 m s^{-1} and a maximum optical path difference (OPD) of 2.8 m, corresponding to a nominal resolution of 0.0037 cm^{-1} (110 MHz). The OPD was calibrated using a stable cw reference diode laser with wavelength $\lambda_{ref} = 1563$ nm. Two out-of-phase comb interferograms were detected at the two outputs of the FTS using an auto-balanced HgCdTe detector (VIGO System, PVI-4TE-6) to reduce the intensity noise [37]. The comb and cw laser interferograms were acquired using a digital oscilloscope (National Instruments, PCI-5922) and home-written LabVIEW™ program. Afterwards, the comb interferogram was resampled at the zero-crossings and extrema of the cw laser interferogram using a home-written MATLAB® program and saved for further analysis.

The comb interferograms were analyzed using the sub-nominal resolution approach [31,33] to achieve comb mode width limited resolution. A total of 200 interferograms with nominal resolution matched to the comb f_{rep} were acquired for a given f_{rep}. Next, the f_{rep} was tuned by 15 Hz and the measurement was repeated. The final spectra were obtained by interleaving 13 individual spectra (each averaged 200 times, 8.3 min acquisition time) recorded with different repetition rates, yielding a sampling point spacing of 11 MHz in the optical domain. The spectra of CH_3I were collected as follows: First, a background spectrum was measured with the evacuated cell for one f_{rep} value. Then, CH_3I was introduced into the absorption cell (either pure or diluted by air) and spectra were recorded for the consecutive f_{rep} steps, each averaged over 200 scans. Each of the steps was normalized to the common background to yield a transmission spectrum, and the absorption coefficient was calculated using the Lambert-Beer law. We note that the same background spectrum could be used for all steps since the background features were broad enough to be unaffected by the shift in sampling point frequencies. To eliminate the residual baseline, the absorption lines were masked and a sum of a fifth order polynomial and a series of sine terms was fit to the remaining spectral structures. The sine frequencies were chosen to match the etalon fringes that were not canceled by the normalization to the background spectrum. Subtraction of the baseline yielded the final absorption spectrum. Finally, the spectra from the consecutive f_{rep} steps were interleaved.

As explained by Rutkowski et al. [33], the sub-nominal resolution approach relies on precise matching of the FTS sampling point spacing, f_{FTS}, to the repetition rate, f_{rep}. While f_{rep} can be stabilized with high accuracy (here 10^{-11} relative accuracy), the accuracy of f_{FTS} is given by the accuracy with which λ_{ref} is known, which, in turn, is limited by the FTS alignment, beam divergence, fluctuations of the refractive index of the air filling the FTS etc. Any

mismatch between f_{FTS} and f_{rep} manifests itself in the measured spectra as a characteristic instrumental line shape (ILS) distortion with odd symmetry and amplitude proportional to that mismatch [33]. Following the procedure described by Rutkowski et al. [33], we iteratively changed the value of λ_{ref} until the ILS became invisible. This was done by fitting a Voigt model to selected isolated lines across the spectrum measured at 0.11 mbar of pure CH_3I and observing the root mean square (RMS) of the fit residual. The optimum value of λ_{ref} corresponds to the minimum residual RMS. From the noise level on the baseline of this spectrum we estimate the remaining relative uncertainty in λ_{ref} to be 4×10^{-8}, which translates to 1.5 MHz uncertainty in the CH_3I line positions. This uncertainty is well below the standard deviation of 10 MHz of the assigned transitions (vide infra).

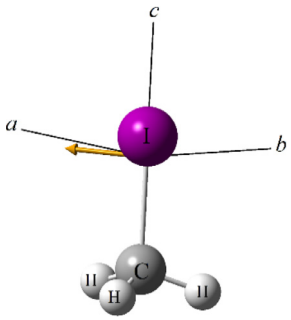

Fig. 3. The molecular structure of CH_3I with the principal axes system. The yellow arrow represents the dipole moment change perpendicular to the principle c-axis as a result of the asymmetric C–H stretch vibration, the ν_4 band.

3. Results and discussion

3.1. High-resolution spectra measurements

Fig. 2(a) presents the high-resolution spectrum of pure CH_3I measured at 0.03 mbar in the region from 2800 cm^{-1} to 3160 cm^{-1}. In this spectral window, CH_3I exhibits a complex ro-vibrational spectrum with three distinct vibrational features, which are all measured simultaneously by our comb-based FTS spectrometer. Panels (b), (c), and (d) show zoomed in parts of the three features, revealing their dense but well-resolved ro-vibrational structure. Note that the spectra in panels (b) and (d) were measured at 0.11 mbar of pure CH_3I, while the spectrum in panel (c) was measured at 0.03 mbar of pure CH_3I [same as in panel (a)], to compensate for the different intensities of the bands. The vibrational features extending from 2800 to 2900 cm^{-1} were investigated by Lattanzi et al. [23] and assigned to several overlapping parallel vibrational bands including the $2\nu_5$, $\nu_3+\nu_5+\nu_6$, and the $2\nu_3+2\nu_6$ bands. The strongest band in this region corresponds to the fundamental ν_1 band of the symmetric C–H stretch (CH_3 s-stretch), centered at 2971 cm^{-1} (note that the strongest lines of the Q branch are saturated). This band was measured and assigned first at a resolution of 0.04 cm^{-1} and later at 0.0054 cm^{-1} by Paso et al. [16,38]. Finally, the fundamental ν_4 band corresponds to the degenerate asymmetric C–H stretch (CH_3d-stretch). This band was first measured by Connes et al. [19] and further investigated by Anttila et al. [20] with a resolution of 0.0054 cm^{-1}. There is no information available about the line intensities or pressure broadening coefficients from previous spectroscopic studies on the three vibrational features in this region. Because of its well-resolved structure, promising for future monitoring applications, the ν_4 band is selected here for further analysis to determine line positions and intensities. As shown in Fig. 2(a), the lower wavenumber tail of the ν_4 band overlaps with the stronger ν_1 band. Therefore, the range from 3010 to 3160 cm^{-1}, which includes the Q sub-branches from $^{P}Q_6$ to $^{R}Q_{11}$, is used for determination of the band parameters in our study.

3.2. Spectral simulations and assignment

Iodomethane was simulated as a symmetric top molecule with an equilibrium structure of the C_{3v} point group (see Fig. 3). Three of the 3N-6 vibrational modes (i.e., ν_1, ν_2, ν_3) are nondegenerate with A1 symmetry, while the remaining ν_4, ν_5, and ν_6 are degenerate with E symmetry.

The spectra were simulated and assigned using PGOPHER [39]. Fig. 4(a) shows an overview of the measured absorption coefficient

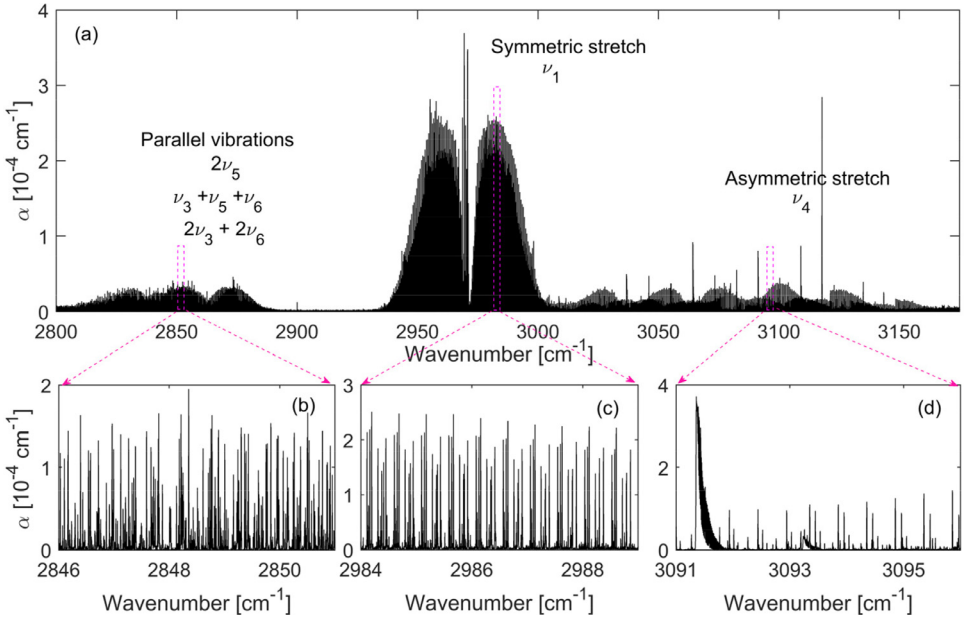

Fig. 2. (a) Overview of the broadband high-resolution spectrum of pure CH_3I measured at 0.03 mbar in the range from 2800 to 3160 cm^{-1}. (b)-(d) The zoomed in spectra showing the dense ro-vibrational structures of the different bands. Spectra in panels (b) and (d) were measured at a pressure of 0.11 mbar to increase the absorption signal due to the lower intensity compared to the ν_1 band in panel (c).

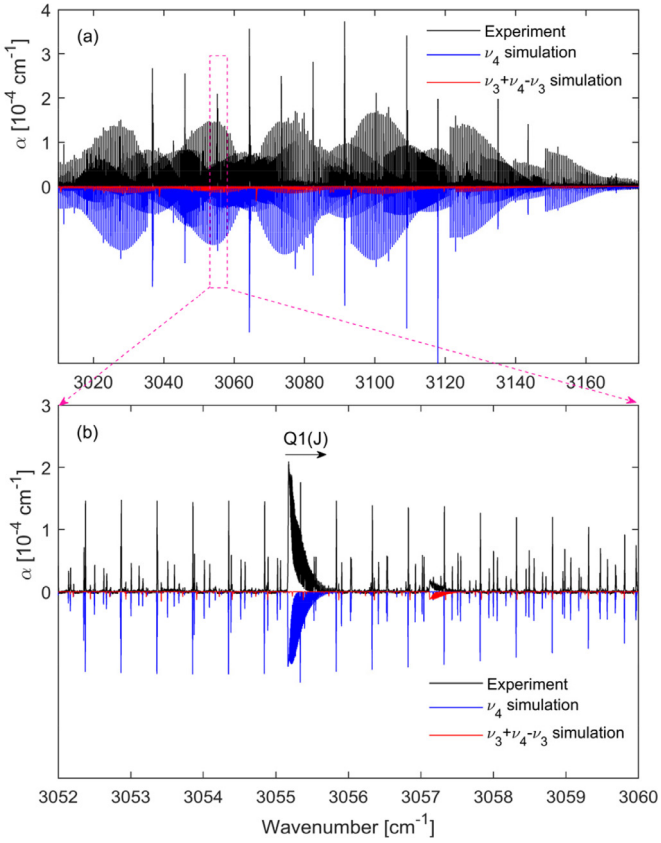

Fig. 4. (a) Measured absorption coefficient, α, of 0.11 mbar of pure CH_3I (black) at 296 K and simulations of the ν_4 band (blue) and the $\nu_3+\nu_4-\nu_3$ hot band (red) obtained from PGOPHER. (b) Zoom in around the $Q_1(J)$ sub-branch of the ν_4 band. The arrow indicates the degradation direction with increasing J.

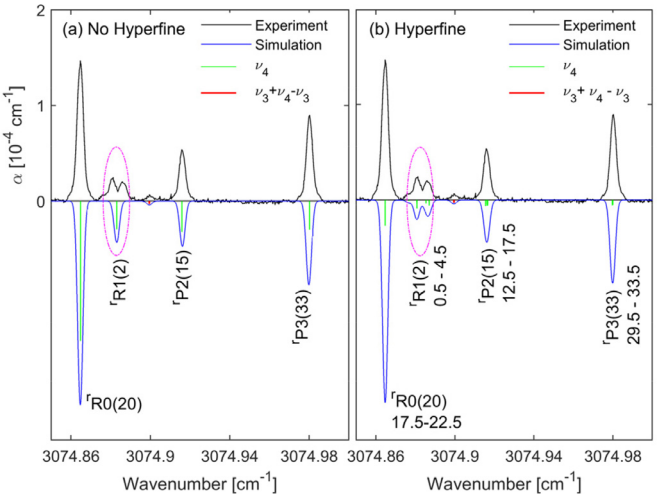

Fig. 5. Measured absorption coefficient, α, of 0.11 mbar of pure CH_3I (black) at 296 K together with line positions of the ν_4 band (green) and the $\nu_3+\nu_4-\nu_3$ hot band (red) without accounting for hyperfine splitting [panel (a)] and after accounting for the hyperfine splitting [panel (b)]. The overall simulation obtained from PGOPHER is shown in blue. The ellipse highlights the ^{r}R1(2) transition with clearly resolved hyperfine sub-components.

of 0.11 mbar of pure CH_3I (black) together with the simulations of the ν_4 band (blue) and the $\nu_3+\nu_4-\nu_3$ hot band (red) obtained from PGOPHER. For the simulations, the input parameters of the ground states were taken from Refs [40,41], while for the upper states they were taken from earlier simulations by Anttila et al. [20]. Starting from the initial simulated spectra, we first assigned the $K(J)$=0 lines near the band origin, then we extended the assignment up to $K = 12$ and $J = 75$ quantum numbers. As shown in Fig. 4, an overall very good match between the experiment and the simulations is obtained. The ν_4 band shows a typical structure of a perpendicular band with $Q_k(J)$ sub-bands degrading towards higher frequencies (i.e., blue shaded), indicating that the term B' - B'' has a small positive value. Panel (b) is an enlarged portion of the spectrum around the $Q_1(J)$ sub-band of the ν_4 band. A series of weak rotational features observed between the main Q-clusters are attributed to the $\nu_3+\nu_4-\nu_3$ hot band, as previously reported by Anttila et al. [20], with intensity equal to ~7.6% of the fundamental ν_4 band, as predicted by the Boltzmann distribution factor.

Because of the large value of the ^{127}I nuclear quadrupole moment (with nuclear spin of 5/2), clusters of hyperfine subcomponents are expected to arise. Such hyperfine structures were previously observed in the microwave region and in the infrared region at 11 μm [14,22]. Fig. 5 shows a fragment of the measured spectrum around 3074.9 cm^{-1}, where clear signs of hyperfine splitting can be observed in the ^{r}R1(2) transition (highlighted in the figure). The experimental data is presented together with simulations without accounting for the hyperfine splitting [panel (a)] and after accounting for it [panel (b)]. To account for the hyperfine splitting, we simulated the spectra as described earlier in this section and included the hyperfine constants of the ^{127}I nuclear quadrupole moment. The nuclear quadrupole constants were fixed to those of the ν_6 band taken from Carocci et al. [14], since the corresponding values for the ν_4 band have not been reported in the literature. As shown in panel (b), the hyperfine subcomponents are clearly visible for the ^{r}R1(2) transition, for which $J \leq 2 \times K$, with splitting of 6.3×10^{-3} cm^{-1}, while for transitions with $J > 2 \times K$ the hyperfine subcomponents show much smaller splitting. For example, hyperfine subcomponents in the ^{r}R0(20) and ^{r}P2(15) transitions are separated by 8.35×10^{-5} cm^{-1} and 1.15×10^{-3} cm^{-1}, respectively. Due to the small splitting of the hyperfine subcomponents for transitions with $J > 2 \times K$ (which is the case for the majority of the strong ro-vibrational transitions of the ν_4 band) and the poorly resolved hyperfine splitting of transitions involving $J \leq 2 \times K$, we have excluded hyperfine structures from spectral assignment. Only transitions with $J > 2 \times K$ are included in the fitting pool, while transitions showing any sign of splitting were excluded from the assignment. On the other hand, we explicitly accounted for the Coriolis and Fermi resonances, which are rather strong and perturb the ν_4 band, as described by Paso et al. [16]. It should be noted that the unresolved hyperfine splitting may result in a slight asymmetry in absorption profiles, and hence affect the accuracy of the reported line intensities and positions.

Overall, 2603 lines were assigned to the ν_4 band with a standard deviation of 0.00034 cm^{-1} (10 MHz), and 831 lines were assigned to the $\nu_3+\nu_4-\nu_3$ hot band with a standard deviation of 0.00084 cm^{-1} (25 MHz). Table 1 compares the number of assigned lines in the two bands, and their corresponding standard deviation, from our comb-based FTS measurement to those based on previous FT-IR work [19,20]. A line list of all transitions assigned in our work is provided in the supplementary materials.

Tables 2 and 3 summarize the parameters of the ν_4 band and the $\nu_3+\nu_4-\nu_3$ hot band obtained from our comb-based FTS measurements at 11 MHz sample point spacing and that of Anttila et al. [20] using standard FT-IR with 162 MHz resolution. Fig. 6 shows the residuals of the least squares fit to the 2603 transitions assigned in our work as a function of J and K quantum numbers using the band parameters from our study [(panel (a)] and from the earlier work of Anttila et al. [20] [panel (b)]. Both simulations used the same set of ground state constants from Refs [40,41]. As shown in this figure, the simulation based on our parameters leads to residuals randomly scattered around zero for transitions up to

Table 1
Current status of the line positions of the ν_4 band and the $\nu_3+\nu_4-\nu_3$ hot band of CH_3I in the C–H stretch region.

Technique			ν_4		$\nu_3+\nu_4-\nu_3$	
	Point spacing	Ref.	Assignments	Std. dev./cm^{-1}	Assignments	Std. dev./cm^{-1}
FT-IR	150 MHz	[19]	500	0.005	–	–
FT-IR	162 MHz	[20]	1850	0.00083	380	0.0013
Comb-FTS	11 MHz	This work	2603	0.00034	831	0.00084

Table 2
Parameters of the ν_4 band of CH_3I obtained from this study compared to that of Anttila et al. [20]. Values in parentheses represent the fit parameter uncertainties at 1σ confidence level.

Constants [cm^{-1}]	This work	Anttila et al. [20]
ν_0	3060.07846(3)	3060.07890(6)
A	5.144014(2)	5.144038(4)
B	0.25033919(3)	0.25034228(7)
$D_J \times 10^7$	2.09373(9)	2.09410(14)
$D_{JK} \times 10^6$	3.3039(5)	3.3139(17)
$D_k \times 10^5$	9.238(2)	9.271(7)
ζ	0.066352(7)	0.06655(10)
$\eta_J \times 10^7$	−5.70(3)	−5.28(8)
$\eta_k \times 10^5$	4.33(2)	4.43(7)
$q_+ \times 10^5$	−1.0102(4)	−1.052(5)
Number of lines	2063	1850
Std. dev	0.00035	0.00083

Table 3
Parameters of the $\nu_3+\nu_4-\nu_3$ hot band of CH_3I obtained from this study compared to that of Anttila et al. [20]. Values in parentheses represent the fit parameter uncertainties at 1σ confidence level.

Constants [cm^{-1}]	This work	Anttila et al. [20]
ν_0	3062.04686(5)	3062.0474(2)
A	5.147074(9)	5.14704(4)
B	0.24852518(2)	0.24852(17)
$D_J \times 10^7$	2.1015(6)	2.09410(14)
$D_{JK} \times 10^6$	2.886(6)	3.0933(12)
$D_k \times 10^5$	7.643(3)	7.830(5)
ζ	0.068644(4)	.06865(6)
$\eta_J \times 10^6$	−1.25(3)	−0.528(8)
$\eta_k \times 10^5$	2.85(2)	4.43(7)
$q_+ \times 10^6$	−9.12(2)	−9.44(5)
Number of lines	831	380
Std. dev	0.00084	0.0013

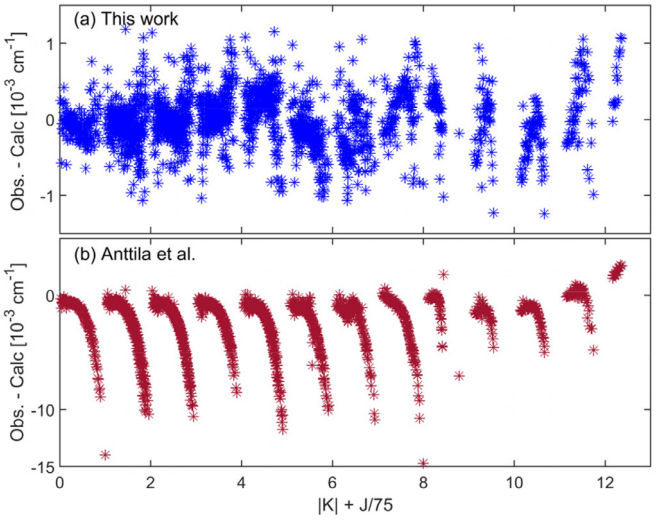

Fig. 6. Fit residuals (observed - calculated) as a function of the upper state K and J quantum numbers of the ν_4 band for (a) our work and (b) using the band parameters of Anttila et al. [20].

$J = 75$ and $K = 12$ quantum numbers, while that based on parameters from Anttila et al. shows larger systematic disagreements for higher J numbers (note the difference in the y-axis scale range in the two panels). Our simulation shows a much smaller deviation for the levels involving higher J values, and hence the reported band parameters from our work are more accurate than from the earlier FT-IR measurements. The large standard deviation for transitions with higher J numbers in Anttila et al. is attributed to the small difference in the reported rotational (A, B) and centrifugal distortion (D_J, D_{JK}, D_K) constants. Such high fit sensitivity to small differences in band parameters is enabled by the high-resolution and precision capabilities of the comb-based Fourier transform spectroscopy.

3.3. Line intensities

The intensities of individual assigned lines of the ν_4 band were found by applying a multispectral fit [42] to selected lines in the spectra measured at four different partial pressures of CH_3I, namely 0.11 mbar, 0.15 mbar, 0.20 mbar and 0.25 mbar, diluted with dry air to a total pressure of 10 mbar. To select these transitions, we first fit Voigt functions to the absorption lines in the spectrum measured at 0.11 mbar of pure CH_3I, same as used for the simulations above, with center frequencies, Lorentzian widths and intensities as free parameters. The fits were applied to the absorption lines separated from the nearest line by more than the Doppler full-width and with peak absorption coefficient exceeding a threshold value of 1×10^{-5} cm^{-1}, excluding those located within the congested Q sub-branches. Second, the retrieved line centers were compared to the line list obtained from the PGOPHER simulations. The closest simulated line was assigned to each fit line if their positions agreed to within 30 MHz, in agreement with the residual shown in Fig. 6(a). Degenerate transitions, which correspond to the A1 and A2 symmetry of each K components of the $K = 3n$ ($n = 1,2,3,\ldots$) levels in the simulation, were treated as one line in the subsequent fitting. Simulated lines that were too weak to be observed and could obstruct correct matching of the simulated and observed absorption lines were filtered out prior to the assignment process. At the end of this process, a total of 838 lines were selected and assigned. Of these, 558 lines separated by at least 10 times the Doppler width (i.e. 960 MHz) from the nearest neighbor were selected for the multispectral fitting.

For the multispectral fit we used a home-written non-linear fitting routine based on the Levenberg-Marquardt algorithm. Each line was modelled as a Voigt line shape with the linestrength and center frequency as fitting parameters. An example of a fit to the ^{r}R9(25) line is shown in Fig. 7(a). The line positions in the spectra measured at a total pressure of 10 mbar were found to be shifted on average by about 2 MHz relative to the spectrum of pure CH_3I measured at 0.11 mbar. This could be accounted for by the pressure shift, but it is close to the uncertainty of 1.5 MHz on the line positions originating from the sub-nominal sampling procedure. The Lorentzian width was fixed to a global value that simultaneously maximized the fit quality on a subset of selected strong lines, which was done for two reasons. First, when the Lorentzian width was fit, its variation across the entire spectrum was random with standard deviation of 1%. Second, we observed

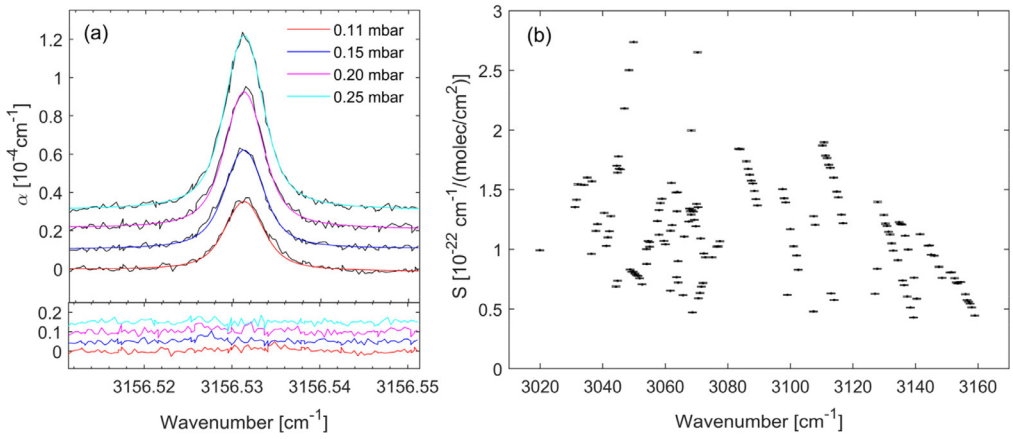

Fig. 7. (a) The multispectral fit to the degenerate ^{r}R9(25) line measured at four different partial pressures of CH_3I (0.11, 0.15, 0.20 and 0.25 mbar) diluted in 10 mbar of dry air. The data is shown in black (offset incrementally upwards for clarity), and the corresponding fits are shown in red, blue, purple and turquoise. The fit residuals are shown in the lower panel, offset vertically. (b) The fitted linestrengths of 157 isolated lines. The error bars display the fit precision. .

a non-negligible instrumental broadening, which we attribute to phase noise of the DFG comb originating from noise on the current driver of the pump diode of the Yb-doped fiber amplifier. Previous measurements on samples of methane, as a test molecule, in the Doppler limit and at known concentrations indicated that the broadening can be modelled by fitting the Lorentzian component of the Voigt profile, and the resulting errors in the fitted line areas were lower than 5%. Since the Lorentzian component of the fit contains an unknown contribution of instrumental origin, we decided not to report the Lorentzian width values. A pressure offset of 19 μbar, attributed to an offset of the pressure sensor, was subtracted from all pressure readings (i.e., the partial and total pressures) as this improved the fit quality. Some of the strongest lines showed signs of saturation in the measurement at 0.25 mbar of CH_3I in 10 mbar of air, which was therefore excluded from the fit for these lines.

We rejected the non-convergent fits, lines with signal to noise ratio lower than 25 at 0.11 mbar of CH_3I in 10 mbar of air (which corresponds to linestrength lower than 0.4×10^{-22} cm^{-1}/molec/cm^{-2}) and fits with quality factor less than 30. The remaining 325 lines were visually inspected to further remove fits that were compromised by interference with weak absorption lines of the ν_4 or the ν_3+ν_4-ν_3 band, and/or by baseline issues due to artefacts not corrected by the baseline removal. We also discarded a dozen lines that appeared anomalously broad, perhaps as a result of unresolved hyperfine splitting. This finally left 157 lines, of which 50 are degenerate transitions with A1 and A2 symmetry. The intensities of those lines are shown in Fig. 7(b). The error bar in the figure shows the precision of the fit, which is on the 0.5% level. We estimate the total uncertainty on the line intensities to be 7%, where 5% comes from the instrumental broadening, 4% from the resolution of the pressure sensor, 1.3% from the uncertainty on the path length in the multipass cell, and 1% from the purity of the CH_3I sample (all summed in quadrature with the fit uncertainty). The experimental line list, with wavenumbers found from fits to the spectrum taken at 0.11 mbar of pure CH_3I and line intensities from the multispectral fits, is reported in the supplementary material. The uncertainty of the center wavenumbers is the combined uncertainty from the fit and the sub-nominal resolution optimization procedure, while the intensities have the 7% relative uncertainty discussed above.

4. Conclusions

Optical frequency comb Fourier transform spectroscopy is introduced as a platform for precision measurements of the lacking high-resolution spectra of trace halocarbons such as CH_3I. The ro-vibrational spectrum of CH_3I in the entire region from 2800 to 3160 cm^{-1} was measured simultaneously, covering three main features of the parallel vibrational overtone and combination bands located around 2850 cm^{-1} and the two fundamental bands: the ν_1 band centered at 2971 cm^{-1}, and the ν_4 band centered at 3060 cm^{-1}. Using the measured ro-vibrational spectrum in the range from 3010 to 3160 cm^{-1} together with the available microwave data [40,41], we simulated the spectra of the ν_4 band and the nearby weak ν_3+ν_4-ν_3 hot band using PGOPHER. New assignment of these bands was introduced and compared to the earlier assignment of Anttila et al. based on standard FT-IR measurements with a resolution of 162 MHz [20]. A least square fit of the assigned transitions to the measured spectrum provided accurate upper state rotational constants of both bands. Overall, we assigned 2603 transitions to the ν_4 band with std. dev. of 0.00034 cm^{-1}, and 831 transitions to ν_3+ν_4-ν_3 hot band with std. dev. of 0.00084 cm^{-1}. The reported upper state band parameters are more accurate than those from the earlier FT-IR-based analysis [20], where 1830 transition with std. dev. 0.00083 cm^{-1} were assigned to the ν_4 band, and 380 transitions with std. dev. of 0.0013 cm^{-1} were assigned to the ν_3+ν_4-ν_3 hot band. The hyperfine splittings due to the ^{127}I nuclear quadrupole moment are clearly observable in the ν_4 band, for the first time, for transitions with $J \leq 2 \times K$, in agreement with recent analysis of the ν_6 band [22]. We also reported intensities of 157 isolated lines in the ν_4 band for the first time, using the Voigt line shape as a model in multispectral fitting. The new line list will serve as a future reference for further investigation of the spectral line parameters for spectral databases such as HITRAN [43] and GEISA [44] as well as a basis for line selection in future monitoring applications of CH_3I.

Declaration of Competing Interest

The authors declare that they have no known competing financial interests or personal relationships that could have appeared to influence the work reported in this paper.

CRediT authorship contribution statement

Ibrahim Sadiek: Conceptualization, Formal analysis, Investigation, Methodology, Project administration, Software, Visualization, Writing - original draft. **Adrian Hjältén:** Data curation, Formal analysis, Investigation, Methodology, Software, Validation, Visualization, Writing - original draft. **Francisco Senna Vieira:** Investigation, Methodology, Software. **Chuang Lu:** Investigation, Methodol-

ogy, Software. **Michael Stuhr:** Investigation. **Aleksandra Foltynowicz:** Conceptualization, Funding acquisition, Methodology, Project administration, Resources, Supervision, Writing - original draft.

Acknowledgements

The authors thank Grzegorz Soboń for providing the polarization maintaining highly nonlinear fiber for the DFG source, Colin Western for providing help with simulating the spectrum in PGOPHER, and Isak Silander for help with setting up the vacuum system and gas supply. This project is financed by the Knut and Alice Wallenberg Foundation (KAW 2015.0159) and the Swedish Research Council (2016–03593).

Supplementary materials

Supplementary material associated with this article can be found in the online version, at doi:10.1016/j.jqsrt.2020.107263.

References

[1] Butler JH, King DB, Lobert JM, Montzka SA, Yvon-Lewis SA, Hall BD, et al. Oceanic distributions and emissions of short-lived halocarbons. Global Biogeochem. Cycles 2007;21:GB1023.
[2] Montzka SA, Reimmann S, O'Doherty S, Engel A, Kruger AK, Sturges W T, et al. Scientific assessment of ozone depletion: global ozone research and monitoring project report. Geneva Switzerland: World Meterological Organization; 2011.
[3] Scientific assessment of ozone depletion: 1998. Global ozone research and monitoring project - Report No 44: World Meterological Organization; 1999.
[4] Chameides WL, Iodine Davis DD. Its possible role in tropospheric photochemistry. J Geophys Res 1980;85:7383–98.
[5] Roth JF. The production of acetic acid. Platin Met Rev 1975;19:12–14.
[6] Clayton GD, Clayton FE. Patty's industrial hygiene and toxicology. 3 editor. New York and Chichester: Wiley; 1991.
[7] Sutton M, Kane SR, Wollard JR. Methyl iodide fumigation of bacillus anthracis spores. Livermore, CA (United States): Lawrence Livermore National Lab.; 2012.
[8] Montreal Protocol on Substances that Deplete the Ozone Layer Final Act 1987. J Environ Law 1989;1:128–36.
[9] Karhu A. Methods to prevent the source term of methyl iodide during a core melt accident. Roskilde, Danmark: NKS; 1999.
[10] . Iodomethane, hazardous substance fact sheet. right to know program. New Jersy Department of Health and Senior Servicies; 1988.
[11] Sadiek I, Shi Q, Wallace DWR, Friedrichs G. Quantitative mid-infrared cavity ringdown detection of methyl iodide for monitoring applications. Anal Chem 2017;89:8445–52.
[12] Wlodarczak G, Boucher D, Bocquet R, Demaison J. The rotational constants of methyl lodide. J Mol Spectrosc 1987;124:53–65.
[13] Dubrulle A, Burie J, Boucher D, Herlemont F, Demaison J. Microwave spectra of methyl chloride, methyl bromide, and methyl iodide in the $\nu_6 = 1$ excited vibrational state. J Mol Spectrosc 1981;88:394–401.
[14] Carocci S, Di Lieto A, De Fanis A, Minguzzi P, Alanko S, Pietilä J. The molecular constants of $^{12}CH_3I$ in the ground and $v_6 = 1$ excited vibrational state. J Mol Spectrosc 1998;191:368–73.
[15] Belli S, Buffa G, Di Lieto A, Minguzzi P, Tarrini O, Tonelli M. Hyperfine level dependence of the pressure broadening of CH_3I rotational transitions in the $v_6 = 1$ vibrational state. J Mol Spectrosc 2000;201:314–18.
[16] Paso R, Horneman VM, Anttila R. Analysis of the ν_1 band of CH_3I. J Mol Spectrosc 1983;101:193–8.
[17] Alanko S. A detailed analysis of the $\nu_2/\nu_5/\nu_3+\ \nu_6$ band system of $^{13}CH_3I$ and $^{12}CH_3I$. J Mol Spectrosc 1996;177:263–79.
[18] Alanko S, Horneman VM, Kauppinen J. The ν_3 band of CH_3I around 533 cm^{-1}. J Mol Spectrosc 1989;135:76–83.
[19] Connes P, Pinard J, Guleachivili G, Maillard J-P, Amit C, Grenier-Besson M-L, et al. Étude de la bande ν_4 de l'iodure de méthyle ICH_3. J Phys France 1972;33:77–84.
[20] Anttila R, Paso R, Guelachvili G. A high-resolution infrared study of the ν_4 band of CH_3I. J Mol Spectrosc 1986;119:190–200.
[21] Yao Z, Zhiye S, Qingshi Z, Cunhao Z. A complete least-squares analysis of a high-resolution laser spectroscopic study of CH_3I ν_5 fundamental. J Mol Spectrosc 1986;115:34–46.
[22] Perrin A, Haykal I, KwabiaTchana F, Manceron L, Doizi D, Ducros G. New analysis of the ν_6 and $2\nu_3$ bands of methyl iodide (CH_3I). J Mol Spectrosc 2016;324:28–35.
[23] Lattanzi F. Parallel vibrational states of CH_3I in the high resolution infrared spectrum from 2770 to 2900 cm^{-1}. J Chem Phys 1990;92:4380–2.
[24] Kwabia-Tchana F, Attafi Y, Manceron L, Doizi D, Vander Auwera J, Perrin A. Line intensities for the ν_6 and $2\nu_3$ bands of methyl iodide ($^{12}CH_3I$). J Quant Spectrosc Radiat Transf 2019;222-223:130–7.
[25] Raddaoui E, Troitsyna L, Dudaryonok A, Soulard P, Guinet M, Aroui H, et al. Line parameters measurements and modeling for the ν_6 band of CH_3I: a complete line list for atmospheric databases. J Quant Spectrosc Radiat Transf 2019;232:165–79.
[26] Boughdiri A, Manceron L, Maaroufi N, Rotger M, Aroui H. Measurements of line intensities for some lines of methyl iodide in the ν_5 and $\nu_3 + \nu_6$ bands. J Quant Spectrosc Radiat Transf 2018;221:147–54.
[27] Barrow GM, McKean DC, Thompson HW. The intensities of absorption bands in the methyl halides. Proc R Soc A 1952;213:27–41.
[28] Dickson AD, Mills IM Jr.. BC. Vibrational Intensities. VIII. CH_3 and CD_3 Chloride, Bromide, and Iodide. J Chem Phys 1957;27:445–55.
[29] Schneider W, Thiel W. Ab initio calculation of harmonic force fields and vibrational spectra for the methyl, silyl, germyl, and stannyl halides. J Chem Phys 1987;86:923–36.
[30] Mandon J, Guelachvili G, Picqué N. Fourier transform spectroscopy with a laser frequency comb. Nat Photonics 2009;3:99–102.
[31] Maslowski P, Lee KF, Johansson AC, Khodabakhsh A, Kowzan G, Rutkowski L, et al. Surpassing the path-limited resolution of Fourier-transform spectrometry with frequency combs. Phys Rev A 2016;93:021802.
[32] Rutkowski L, Johansson AC, Zhao G, Hausmaninger T, Khodabakhsh A, Axner O, et al. Sensitive and broadband measurement of dispersion in a cavity using a Fourier transform spectrometer with kHz resolution. Opt Express 2017;25:21711–18.
[33] Rutkowski L, Masłowski P, Johansson AC, Khodabakhsh A, Foltynowicz A. Optical frequency comb Fourier transform spectroscopy with sub-nominal resolution and precision beyond the Voigt profile. J Quant Spectrosc Radiat Transf 2018;204:63–73.
[34] Soboń G, Martynkien T, Mergo P, Rutkowski L, Foltynowicz A. High-power frequency comb source tunable from 2.7 to 4.2 μm based on difference frequency generation pumped by an Yb-doped fiber laser. Opt Lett 2017;42:1748–51.
[35] Silva de Oliveira V, Ruehl A, Masłowski P, Hartl I. Intensity noise optimization of a mid-infrared frequency comb difference-frequency generation source. Opt Lett 2020;45:1914–17.
[36] Khodabakhsh A, Ramaiah-Badarla V, Rutkowski L, Johansson AC, Lee KF, Jiang J, et al. Fourier transform and Vernier spectroscopy using an optical frequency comb at 3–5.4 μm. Opt Lett 2016;41:2541–4.
[37] Foltynowicz A, Ban T, Masłowski P, Adler F, Ye J. Quantum-noise-limited optical frequency comb spectroscopy. Phys Rev Lett 2011;107:233002.
[38] Paso R, Anttila R, Guelachvili G. Perturbations in the ν_1 band of CH_3I. J Mol Spectrosc 1990;140:46–53.
[39] Western C. PGOPHER version 10.1.. University of Bristol Research Data Repository; 2018 http://pgopher.chm.bris.ac.uk *accessed* 10 *January* 2019.
[40] Mallinson PD. The microwave spectrum of CH_2DI. J Mol Spectrosc 1975;55:94–107.
[41] Boucher D, Burie J, Dangoisse D, Demaison J, Dubrulle A. Doppler-free rotational spectrum of methyl iodide. Nuclear quadrupole, spin-rotation and nuclear shielding tensors of iodine. Chem Phys 1978;29:323–30.
[42] Benner DC, Rinsland CP, Devi VM, Smith MAH, Atkins D. A multispectrum nonlinear least squares fitting technique. J Quant Spectrosc Radiat Transf 1995;53:705–21.
[43] Gordon IE, Rothman LS, Hill C, Kochanov RV, Tan Y, Bernath PF, et al. The HITRAN2016 molecular spectroscopic database. J Quant Spectrosc Radiat Transf 2017;203:3–69.
[44] Jacquinet-Husson N, Armante R, Scott NA, Chédin A, Crépeau L, Boutammine C, et al. The 2015 edition of the GEISA spectroscopic database. J Mol Spectrosc 2016;327:31–72.